HHS Public Access

Author manuscript

ACS Chem Biol. Author manuscript; available in PMC 2023 May 20.

Published in final edited form as:

ACS Chem Biol. 2022 May 20; 17(5): 1073–1081. doi:10.1021/acschembio.1c00912.

Identification and characterization of small molecule IRF3-dependent immune activators for pharmaceutical development

Marie H. Foss[1], **Susan L. Stevens**[1], **Haihong Jin**[2], **Elyse M. Allen**[3], **Dylan Nelson**[4], **Victor DeFilippis**[5], **Aaron Nilsen**[2], **Mary P. Stenzel-Poore**[3]

[1]Neuralexo, INC. 4640 SW Macadam Ave Suite 120, Portland, OR USA.

[2]Medicinal Chemistry Core, Oregon Health & Science University. Portland, OR USA.

[3]Molecular Microbiology and Immunology Department, School of Medicine, Oregon Health & Science University. Portland, OR USA.

[4]High-Throughput Screening Services Laboratory, College of Pharmacy, Oregon State University. Corvallis, OR USA.

[5]Vaccine and Gene Therapy Institute, Oregon Health & Science University. Portland, OR USA.

Abstract

We sought to develop a small molecule activator of interferon regulatory factor 3 (IRF3), an essential innate immune transcription factor, that could potentially be used therapeutically in multiple disease settings. Using a high-throughput screen, we identified small molecule entities that activate type I interferon response, with minimal off-target NFκB activation. We identified 399 compounds at a hit rate of 0.24% from singlicate primary screening. Secondary screening included the primary hits and additional compounds with similar chemical structures obtained from other library sources and resulted in 142 candidate compounds. Hit compounds were sorted and ranked to identify compound groups with activity in both human and mouse backgrounds to facilitate animal model engagement for translational development. Chemical modifications within two groups of small molecules produced leads with improved activity over original hits. Further, these leads demonstrated activity in ex vivo cytokine release assays from human blood and mouse bone marrow-derived macrophages. Dependence on IRF3 was demonstrated using bone marrow-derived macrophages from IRF3 deficient mice, which were not responsive to the molecules. To identify the upstream pathway leading to IRF3 activation, we used a library of CRISPR knockout cell lines to test key innate immune adaptor and receptor molecules. These studies indicated a surprising TRIF-dependent, but TLR3/4-independent mechanism of IRF3 activation.

Graphical Abstract

Corresponding author: Marie H. Foss, mfoss@caymanchem.com.

Conflict of interest

SLS and MPS own equity shares in Neuralexo, INC.

Supporting Information Available: Additional information regarding the chemical structures and corresponding in vitro activity of all small molecules tested in the course of this effort are available in the excel file. The methods for synthesis of small molecules are available in the word document. This material is available free of charge via the Internet.

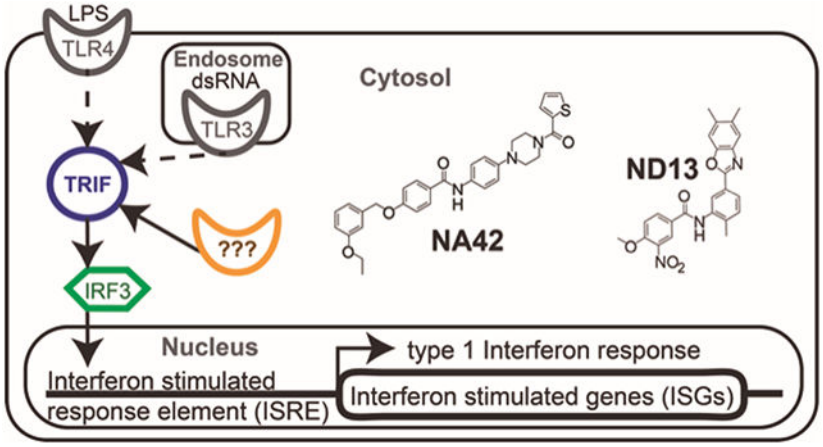

The innate immune system detects and disperses information from the extra- and intracellular environment to mount coordinated responses intended to defend cells, tissues, and the greater organism against threats.[1, 2] Interferon regulatory factor 3 (IRF3) is a key transcriptional regulator of the innate immune response that has shown therapeutic potential in vaccine development,[3, 4] antivirals,[4-6] and cancer.[7, 8] IRF3 activators can act as adjuvants in vaccines to increase immune system responses[4] and mobilize the antiviral response more efficiently to suppress viral infections.[9] Interestingly, IRF3 has been shown to affect tumor growth and mobility in cancer.[8, 10] Animal studies have demonstrated that IRF3 agonists can directly inhibit tumor growth,[11] and induce recruitment of beneficial CD8+ Tcells.[12] In addition, IRF3 was shown to suppress glioblastoma tissue invasion in both ex vivo and in vivo models using human derived glioblastoma cell lines.[8]

Molecular mechanisms associated with induction of IRF3 include engagement of membrane bound Toll-like receptors (TLRs) and cytosolic retinoic acid-inducible gene I (RIG-I) like receptors (RLRs), both key biosensors for innate immunity.[13, 14] TLR3 and TLR4 can signal from the endosome through adaptor molecule TIR-domain-containing-adapter-inducing interferon-β (TRIF) to recruit and activate IRF3. RLRs are cytosolic RNA sensors that include 3 family members: RIG-I, melanoma differentiation-associated protein 5 (MDA5) and laboratory of genetics and physiology 2 (LGP2). The key adaptor molecules associated with RLR activation of IRF3 are stimulator of interferon genes (STING) and interferon-β promoter stimulator 1(IPS1).

Our goal was to develop a pharmacological activator of IRF3 that would have the translational potential for development as a therapeutic against varying diseases. We performed a high-throughput screen to identify small molecule candidates, using an Interferon Stimulated Response Element (ISRE) reporter construct. Activators of IRF3 have the potential to also activate NFκB, which can lead to a variety of inflammatory mediators, including TNFα, which could have significant off-target effects.[15] To minimize inflammatory effects associated with NFκB, we performed a counterscreen in parallel to the measurement of ISRE activation using an NFκB reporter construct. We also prioritized compounds with activity in both human and mouse macrophage models to promote translational efforts. Currently available small molecule agonists of IRF3 have struggled

with a variety of issues, including species specific differences in the innate immune response that have slowed translation between model species.[16]

RESULTS and DISCUSSION

Primary screen and statistical analysis of hits.

In total, we screened 168,256 small molecules in singlicate for their ability to activate ISRE with minimal activation of an NFκB promoter. We used differentiated THP1 Dual cells, a human monocyte cell line developed by InvivoGen to assess ISRE and NFκB activity simultaneously. We evaluated each compound in the library for activation of ISRE and NFκB via two different metrics, one relative to internal plate controls that we refer to as the percent activation (PA) method (Figure 1a) and the other relative to the average sample signal or the Zscore method.[17] The PA method takes into account the performance of each assay plate in terms of signal output and prevents inflation or absence of hits in plates where the signal strength of controls was significantly higher or lower than the average plate in a batch. Alternatively, the Zscore method assumes the vast majority of compounds have no effect on signal and simply evaluates whether an individual compound output is outside of this background. We applied these methods to batches of plates (40/batch) screened at the same time and used a cutoff of 6σ above the batch mean for ISRE activation as an indication of a positive response.

Validation of singlicate screen hits and similarity searched compound activity.

In our validation screen, we wanted to confirm hits from the singlicate screen and assess cross species activity. We advanced 399 tentative hits from our primary screen that met the greater than 6σ cutoff criteria. Many of these tentative hits shared chemical scaffolds or functional groups, allowing us to define 4 distinct chemical families/clusters of potential interest, which we denoted as NA, NB, NC and ND. We used example compounds from these hit clusters to perform similarity searches of compound library materials from the Oregon State University High-throughput screening services laboratory. We selected 98 additional compounds not present in our original screen to include for validation, resulting in a total of 497 compounds (399 original hits + 98 structurally similar compounds). We assessed the 497 candidate molecules in duplicate in the human differentiated THP1 Dual cells, and in mouse J774 macrophage-like Dual cells with the same stably transfected reporter constructs (InvivoGen). We included blank wells distributed across the compound plates for establishment of background signal to develop the cut-offs for confirming hits. We again set a cut-off for ISRE activation at 6σ above the background average. In addition, for the counterscreen, we set a cut-off of 2σ as an indication of NFκB activation (Figure 1b). We calculated a fold (ISRE/NFκB) and difference (ISRE-NFκB) score for hits with NFκB-associated SEAP activation of greater than 2σ. Compounds were required to produce twice as much ISRE to NFκB signal or produce a difference of at least 50% ISRE activation relative to NFκB. Examining both the fold and difference scores prevented the possible elimination of strong ISRE activators. Of the 497 compounds evaluated in the validation screen, 142 met the criteria for confirmed ISRE activation in the human line.

Of the 142 confirmed hits, 135 were originally identified from the singlicate primary screen and 7 were selected from the similarity searches. The identification of 7 positive hits from the manually selected compounds demonstrates that the structure clustering of our primary hits afforded viable activity information. We determined that the overall confirmation rate of the PA method was 42% and the Zscore method was 34%. The compounds identified as hits in both methods had a confirmation rate of 52%. Sixty-nine of the confirmed ISRE active compounds also demonstrated low NFκB activation, which prioritized them for closer follow-up. Importantly, of these 69 compounds, we found that 5 are active in the mouse macrophage model. The cross-species active hits allow for additional testing and development to occur using mouse model systems.

Evaluation and ranking for structure activity relationships (SAR).

To rank each compound hit, we performed dose-response measurements to establish a 50% maximally effective concentration (EC_{50}) value for ISRE and NFκB activation in the human THP1 Dual and mouse J774 Dual cell lines (Table 1 and supplemental information). We also determined the 50% cytotoxic concentration (CC_{50}) value for these cell lines to prioritize compounds with minimal toxicity relative to the concentration effective for ISRE activation. In addition, as information was generated from the original hits, we prepared or obtained, from commercial sources, additional analogs from each of the 4 chemical families for SAR evaluation. Two lead families, NA and ND demonstrated the highest potential for development and were carried forward. During SAR we found that the maximum relative percent ISRE activation varied between compounds, suggesting binding of different targets or differential access to the target for activation of ISRE (Figure 2). For example, all compounds were normalized to the maximum response achievable with lipopolysaccharide (LPS). NA42 (198% of LPS maximum) and ND13 (188% of LPS maximum) were able to induce ISRE to greater levels than LPS, but the maximum induction induced with ND95 (52% of LPS maximum) is about half of the LPS level; the differences between ND13 and ND95 result in significantly less total ISRE activation. We considered these values as well as molecular weight and clogP to establish leads for introduction to ex vivo studies. As a positive control for ISRE activation in mouse cells, we used the known small molecule, anti-tumor STING agonist DMXAA, which is inactive in human cells. NA42 (3.6 μM EC_{50}) and ND13 (1.0 μM EC_{50}) are about five to twenty times more active, respectively, than DMXAA (24 μM EC_{50}) based on ISRE activation; however, both compounds have higher clogP values (Figure 2). ND95 in comparison to DMXAA shares a similar clogP (3.7 versus 3.22, respectively) and has a lower EC_{50} of 0.6 μM; however, ND95 loses a significant amount of total ISRE activation (52% of LPS maximum). Further efforts will be required to determine if improvements to the drug-like properties of the compounds can be achieved while maintaining robust activity for both EC_{50} and total ISRE activation.

SAR observations.

The active compounds within the NA series have a piperazine with an amide linkage to a thiophene ring attached at R_2 on ring B (Figure 3a, supplemental materials). Active compounds typically carry a benzyloxy group at R_5. Additional modifications to the benzyloxy group at R_5 can be made by addition of chemical groups to the ring, but the methoxy linker does not appear to allow for additional substitution. Replacement of ring

A with halogenated naphthalenes can produce human active compounds, however, they are inactive in the mouse background. Introduction of a nitrogen to ring A at positions 2 or 3 also show species specific effects, with both modifications being active in the human background. However, with a nitrogen at position 2 of ring A, nearly all mouse activity was lost. With a nitrogen at position 3 of ring A, the activity in the mouse line was retained. The lead compound pursued in mechanism of action studies from this series was NA42 (Figure 3b).

The active compounds within the ND series utilize position 3 of ring B, where the major feature at R4 is the requirement of a nitro group (Figure 3a, supplemental material). There is also a strong preference for a substituent at R_3 and R_5. With the nitro group at R_4, the preference at R_5 is for a methoxy as other substitutions lead to activity loss. The main lead compound pursued in the mechanism of action studies from this series was ND13 (Figure 3b). Swapping of ring A or B between the NA and ND series has thus far resulted in inactive compounds, suggesting they bind different targets or different binding sites on the same target, which results in divergent downstream effects.

IRF3 target activation.

To determine whether our lead compounds, NA42 and ND13 could elicit IRF3 dependent cyto/chemokine responses, we isolated bone marrow-derived macrophages (BMDM) from wildtype and IRF3 deficient ($IRF3^{-/-}$) mice. As controls we used the IRF3 agonist, DMXAA[16] and IFNβ, which can induce cyto/chemokine production in an IRF3 independent manner through the IFN receptor.[18] Cells were treated for 24 hours with the compounds at a dose that gave maximum ISRE activation in our reporter cells with minimal cell death, which for DMXAA required 22 μM and a quarter of that amount (6.25 μM) for both NA42 and ND13. Supernatant was collected and secreted cyto/chemokines were measured using a panel of 21 antibodies, either via an ELISA or Luminex assay. ND13 induced production of IP10, IL6, TNFα, Rantes and Mip1α in BMDMs isolated from wildtype, but not from $IRF3^{-/-}$ mice indicating that induction of these cyto/chemokines was IRF3 dependent. ND13 also significantly increased levels of CXCL1, however, the increase was not completely abrogated in $IRF3^{-/-}$ BMDMs, suggesting that part of the increase in CXCL1 was IRF3 independent (Figure 4a).

NA42 also demonstrated IRF3 dependent induction of IP10, IL6, TNFα and Rantes similar to ND13, although the increases in TNFα and Rantes were both significantly lower in the NA42 treated cells (Figure 4a). Interestingly, unlike ND13, the NA42 induction of CXCL1 was completely IRF3 independent, and there was no significant increase in Mip1α suggesting a difference in the mechanism of action for these two compounds.

As expected, DMXAA induced the chemo/cytokines in an IRF3 dependent manner with no induction detected in the $IRF3^{-/-}$ cells. IFNβ induced IP10 and CXCL1 in both wildtype and $IRF3^{-/-}$ BMDMs demonstrating that IRF3 independent induction of these cyto/chemokines was possible in the $IRF3^{-/-}$ cells (Figure 4a).

To determine if NA42 and ND13 could induce a cyto/chemokine response in human cells, we used whole blood-derived human macrophages. Importantly, both NA42 and ND13

elicited significant increases in levels of secreted IP10 (Figure 4b). These data indicate that the lead compounds from the NA and ND series demonstrate promise for production of drug-like small molecule activators of ISRE.

Biomolecular pathway engagement.

IRF3 is a central transcription factor associated with the innate immune response and is downstream of numerous adaptor proteins and receptors. To determine potential upstream targets of our lead compounds we used a panel of telomerase-transduced human foreskin fibroblasts (THF) ISRE-reporter driven cells that were deficient in either TRIF, IPS1 or STING, key adaptor proteins. We included control treatments for each of the signal pathways. LPS binds TLR4, which signals through TRIF to activate IRF3.[1] PolyIC binds TLR3, also using the adapter molecule TRIF to activate IRF3.[19] The molecule G10 signals through STING and Sendai virus is dependent on IPS1 for activation of IRF3 induced gene transcription.[20, 21] Both NA42 and ND13 induced robust activation of the ISRE-dependent reporter in the IPS1 and STING knockout lines indicating that these adaptors are not required for ISRE induction (Figure 5a). In the TRIF knockout cells, NA42 and ND13 activation was significantly attenuated in comparison to wildtype activation, indicating that NA42 and ND13 require TRIF to induce ISRE-dependent transcription.

To further assess the relevant pathways associated with NA42 and ND13 activation of IRF3 we examined the two receptors that have TRIF as an adapter molecule, TLR3 and TLR4. Surprisingly, we found that NA42 and ND13 were both able to induce robust ISRE reporter transcription in THF cells deficient in either of these receptors, indicating that they are not required for the TRIF- and IRF3- dependent induction of the ISRE reporter by these molecules. The ISRE activation activity of NA42 and ND13 is dependent on TRIF in THP1 cells as well (Figure 5b). We confirmed that the reporters responded similarly to stimulation with Sendai virus and IFNβ for the THP1 wildtype and THP1 TRIF knockout line, with the exception of the TRIF-dependent agonist LPS (Figure 5c). This suggests that another TRIF-dependent target or receptor is involved in NA42 and ND13 activation of ISRE gene transcription, or that the compounds are acting directly on TRIF.

A potential biological relevance of the active compounds is their similarity to nitrated or oxidized versions of tyrosine and tryptophan. The cytokine response could be a result of sensing products of reactive nitrogen or oxygen species by the cell as a damage signal, or nitration as a posttranslational modification for normal innate immune system pathway signaling.[22] The production of nitric oxide has also been suggested to be a contributor to the effectiveness of DMXAA and derivatives.[23] A major nitrated molecule produced biologically is 3-nitrotyrosine, which is similar to ring A for the ND series. For tryptophan, a common nitrated version is 6-nitrotryptophan. An example of oxidized tryptophan is hydropyrroloindole; it is interesting to note that we observed tetrahydrocarbazoles as hits in the primary screen.[24] This could also explain the activity of the halogenated naphthalenes from the NA series, as they may be biologically relevant through steric and electrostatic similarity to 6-nitrotryptophan. Further work will be required to determine if these features drive ISRE activation and whether derivatives based more directly on these elements can produce therapeutics.

Given the potential for effects on protein abundance by the small molecule treatments, we measured the amount of IRF3 and NFκB in cells treated with NA42 and ND13 (Figure 6a, b). In THP1-Dual cells stimulated with LPS or doses of our lead compounds, we observed increases in both IRF3 and NFκB levels occurring within 1 hour of treatment (Figure 6c, d). The effects on IRF3 and NFκB were dose dependent for both NA42 and ND13. Additional work will be required to evaluate IRF3 phosphorylation and translocation of this transcription factor into the nucleus. In addition, the direct target(s) of NA42 and ND13 remain to be determined, as they could modulate a variety of partners that interact with IRF3 and/or TRIF in their regulation and function. For example Pin1 has been shown to negatively regulate IRF3, with suppression of Pin1 resulting in enhanced IRF3 dependent induction of IFNβ.[25] Thus, NA42 and/or ND13 may enhance IRF3 activity indirectly through interaction with Pin1 or other regulators or IRF3 and/or TRIF. Overall, our data indicates that the target(s) of the compounds regulates either the production or degradation of the members of this innate immune pathway.

This research identified new small molecule entities that result in activation of IRF3, a transcription factor of interest for the development of antivirals, vaccine adjuvants, as well as cancer therapeutics.[4, 8, 9] These compounds have the potential to not only activate typical antiviral responses, but also act as adjuvants in vaccine preparations. In addition, activation of IRF3 has been shown to slow the growth and invasion of glioblastoma,[8, 26] suggesting a possible role in cancer therapies potentially independent of innate immune responses.

METHODS

Primary screen.

Prior to the primary screen we performed a pilot screen in triplicate on a 2560 compound library (The Spectrum Collection, MicroSource Discovery Systems, Inc.) containing therapeutics of known activity and natural products to develop, optimize, and evaluate assay performance (data not shown). For the primary screen 168,256 small molecules, from the Oregon Translational Research and Development Institute (OTRADI) Small Molecule Library, were screened in singlicate. This library was purchased from SIGA Technologies in 2014 and is made up of compounds from the ChemBridge DIVERSet™-CL library, the ChemBridge CORE Library, and two focused antiviral libraries from Life Chemicals and ChemDiv. Compounds were screened in differentiated THP1 Dual cells (InvivoGen), a human monocytic reporter cell line with secreted Lucia luciferase activity coupled to ISRE activation via an ISG54 minimal promoter driven by five ISREs. Secreted embryonic alkaline phosphatase activity is controlled by an IFNβ minimal promoter driven by five copies of the NFκB consensus transcriptional response element and three copies of the c-Rel binding site. THP1 Dual cells were maintained in RPMI 1640 (Gibco) supplemented with 10% fetal bovine serum (Hyclone), 100 U/mL Normocin (InvivoGen), and 50 U/mL PenStrep (Gibco) between a density of $7•10^5$-$2•10^6$ cells/mL. Every other passage, media was supplemented with 5 U/mL Blasticidin and 100 U/mL Zeocin to maintain the expression constructs (InvivoGen). For screening assays, cells were seeded on flat-bottom 384-well plates (Greiner) at a density of $2.5•10^4$ cells/well in media containing 5 ng/mL phorbolmyristic acid (PMA) to differentiate cells. After 48 hours, wells were washed three

times with phosphate buffered saline (PBS) to remove PMA. Plates were reloaded with media without PMA and treatments added. As a positive control, LPS in dimethylsulfoxide (DMSO) was used at a final concentration of 313 ng/mL, a concentration determined to be maximally activating with minimal cell loss. Test compounds from chemical library plates were added to a final concentration of 10 μM using a Sciclone robotic liquid handling device fitted with a 384-well pin tool.

Plates were incubated for 24 hours, then 10 μL of supernatant from each well was transferred, using a Sciclone robotic liquid handling device fitted with a 96-well pipette transfer head, into a white, flat-bottom 384-well plate for luminescence readout and a black-walled, clear flat-bottom 384-well plate for absorbance readout. To the white readout plate, 10 μL QUANTI-Luc reagent (InvivoGen) was added to each well. Plates were agitated for 30 seconds prior to a 0.1 s integration luminescence readout. To the black clear bottom plates, 20 μL QUANTI-Blue reagent (InvivoGen) was added to each well. Plates were agitated for 30 seconds and then incubated at 37°C for 1 h prior to absorbance readout at 630nm.

Statistical analysis of hits.

Data was analyzed in batches of 40×384 well plates, which represents the number of plates performed in parallel during a given week of the primary screen. Two different metrics were used to evaluate each compound in the library for activation of ISRE and NFκB. The two methods were used to take into account both in-plate control activation as well as background signal strength across the screen.[17] The Percent Activation (PA) method calculates the average and standard deviation of the percent activation of the samples compared to internal control included on each plate. Compounds were considered hits if their percent ISRE activation exceeded 6σ above the mean for the batch (Figure 1a). The PA method resulted in 416 hits (0.25% hit rate). Of those 416 hits, 231 were classified as weak NFκB activators (Figure 1b).

In the Zscore method, the raw signal mean for each individual plate was subtracted from individual sample signals and divided by the standard deviation, which resulted in each compound receiving a numerical value in multiples of σ. Compounds were considered ISRE activators if their Zscore ≥ 6σ, which resulted in 478 hits (0.29%). Of those 478 hits, 290 were classified as weak NFκB activators. Although both analysis methods identified a similar number of hits, only 122 compounds (~30%) were shared between the two methods. A counterscreen was performed on hit compounds identified from both the PA and Zscore methods with an NFκB activation 2σ above baseline averages. Two values were calculated to determine if a compound remained in the hit list; compounds remained hits with an ISRE/NFκB ratio >2 or an ISRE-NFκB normalized activation difference of at least 50%.

As the initial screen hits were from singlicate measurements, a validation screen was performed on compounds identified as hits in either one of the analysis methods. This gave a combined unique hit count of 399 or 0.24% of queried compounds to carry forward for reevaluation. Identified hits were selected from the original library plates and transferred to two new compound plates using a Hamilton robotic liquid handling device for validation screening. Interestingly, a review of the chemical structures of the hits identified

at least 4 distinct clusters of compounds with similar scaffolds and chemical features. As we screened a portion of the small molecules available at the Oregon State University High-throughput screening services laboratory, a similarity search was performed using a Tanimoto coefficient of 0.8 in the Dotmatics software on the complete small molecule library, including both known FDA approved drugs and other commercially available chemical diversity libraries. A total of 98 compounds with structural similarity to the primary screen hits were included in the validation screen.

Cross-species evaluation and orthogonal screen.

To identify compounds with cross-species activity we screened our candidate compounds in J774 Dual cells (InvivoGen), a mouse macrophage cell line with the same reporter constructs as the THP1 Dual cells. J774 Dual cells were maintained in DMEM (Gibco) supplemented with 10% fetal bovine serum (Hyclone), 100 U/mL Normocin (InvivoGen), and 100 U/mL PenStrep (Gibco) between a density of $2.5 \bullet 10^4$-$2 \bullet 10^5$ cells/cm^2. Every other passage, media was supplemented with 10 U/mL Blasticidin and 100 U/mL Zeocin to maintain the expression constructs. For screening assays, cells were seeded on flat-bottom 384-well plates (Greiner) at a density of $2.5 \bullet 10^4$ cells/well. After 24 hours of incubation, plates were washed three times with PBS. Plates were reloaded with media and treatments added in parallel to the THP1 Dual validation assay using a Sciclone robotic liquid handling system fitted with a 384-well pin tool. After incubation with treatments for 24 hours, 20 μL of supernatant from each well was transferred into a white, flat-bottom 384-well plate for luminescence readout and a black-walled, clear flat-bottom 384-well plate for absorbance readout. Readout methods for the J774 Dual supernatants were similar to the THP1 Dual cells with the exception of increasing the QUANTI-Blue reagent to 40 μL per well.

SAR compounds, evaluation and ranking.

Following primary and orthogonal screening, we obtained new stocks of our candidate compounds as well as additional small molecule analogs for SAR from commercial vendors or via synthesis by the OHSU Medicinal Chemistry Core (supplemental materials). Freshly synthesized or purchased candidate compounds were rescreened in the THP1 Dual and J774 Dual cell line assays with a 10-point dose response curve in triplicate for each compound. Signal strength was normalized for each measurement to internal plate controls and activation curves were fit using Prism to establish half maximal effective concentration (EC_{50}) values for ISRE and NFκB activation in each cell line. The 50% cytotoxicity level (CC_{50}) value for each candidate compound was determined by treatment of the dose-response tissue culture plates with CellTiter-Glo (Promega) according to manufacturer recommendations.

Mice.

C57BL/6 mice (male, 8-12 weeks) were purchased from Jackson Laboratories (West Sacramento, CA). IRF3$^{-/-}$ mice were obtained from RIKEN BioResource Center (Tsukuba, Japan) and have been backcrossed > 8 generations onto C57BL/6. Verification of IRF3 deficiency for each animal used in experiments was done by PCR using IRF3 specific primers. All mice were housed in an American Association for Laboratory Animal Care-approved facility. Procedures were conducted according to Oregon Health & Science

University, Institutional Animal Care and Use Committee, and National Institutes of Health guidelines.

Mouse bone marrow derived macrophages.

Bone marrow-derived macrophages were isolated from C57BL/6 or IRF3$^{-/-}$ mice. In brief, bone marrow was obtained by removing the condyles of the femur and tibia bones with surgical scissors and flushing the marrow cavity with DMEM using a syringe. The collected cell suspension was passed through a 40 μm nylon filter, centrifuged and the resulting cell pellet was resuspended in ACK lysis buffer (ThermoFisher). Following red blood cells lysis, cells were washed in PBS and resuspended in DMEM with 20% L-cell conditioned media (LCCM) and seeded at a plated density of 5•10^5 cells/cm2 for differentiation. After 3 days, media was quickly removed to eliminate non-adherent cells and fresh DMEM with 20% LCCM supplement was added. Cytokine release experiments were performed on day 7.

Human monocyte derived macrophages (MDMs).

Human monocyte derived macrophages (MDMs) were derived from monocytes isolated from deidentified whole blood obtained from the Oregon Clinical and Translational Research Institute (OCTRI) Volunteer Registry with Histopaque (Sigma, Cat. 10771) according to manufacturer recommendations. After isolation, cells were plated at 1.5•10^6 cells/cm^2 first with monocyte attachment media (VWR, Cat.10172-398) for 1.5 hours at 37°C with 5% CO_2. Media was replaced on the adherent cells with 10% (v/v) giant cell tumor-conditioned complete macrophage base media (VWR, Cat. 10172-410). Cells were harvested on day 7 using macrophage detachment solution (VWR, Cat. 10175-308) and replated on treatment plates at 6•10^5 cells/cm^2. Cytokine release experiments were performed on day 8.

Cytokine release profile.

Adherent mouse and human macrophages were incubated at 37°C with 5% CO_2 with compound treatments for 24 hours and supernatant collected. For the mouse samples, cytokines were measured using a mouse specific Luminex Assay (Invitrogen, Cat. EPX020-26090-901; GM-CSF, IFNγ, IL1b, IL12p70, IL13, IL18, IL2, IL4, IL5, IL6, TNFα, Eotaxin, Gro-alpha/KC, IP10, Mcp1, Mcp3, Mip1a, Mip1b, Mip2, Rantes) according to manufacturer guidelines. IP10 was measured from the human macrophage supernatant using a human specific CXCL10/IP10 ELISA (R&D Systems Cat. DIP100) according to manufacturer guidelines.

Biomolecular pathway engagement.

A small library of THF cell lines carrying an ISRE-coupled reporter were constructed that lack either TRIF, STING, IPS1, TLR3 or TLR4 via CRISPR as described previously.[24] Cells were seeded at 5•10^4 cells/well in 384 well plates 24 hours prior to treatment with candidate compounds. Cells were incubated for 8 hours and supernatants collected for ISRE activation, which was measured using SteadyGlo reagent (VWR, Cat. PAE2520) per the manufacturer recommendations.

Automated western blots.

THP1-Dual cells were treated as indicated for 1 hour prior to preparation of protein extracts with M-PER mammalian protein extraction reagent (Thermo Scientific, Cat. 78501) containing 1x Halt protease and phosphatase inhibitor cocktail (Thermo Scientific, Cat. 1861281). Protein concentrations were quantified using a standard Braford assay. An automated western blot method was performed on samples using a 12–230 kDa 25 lane plate (ProteinSimple, Cat. PS-MK15) in a ProteinSimple Wes Capillary Western Blot analyzer according to the manufacturer's instructions, except the primary antibody incubation was increased to 45 minutes. Primary antibodies used were IRF3 (Cell Signaling, Cat. 4302) diluted 1:25, NFκB (Abcam, Cat. ab32536) diluted 1:100, and GAPDH (Cell Signaling, Cat. 2118) diluted 1:500. Diluent was Antibody Diluent 2 (Protein Simple).

Supplementary Material

Refer to Web version on PubMed Central for supplementary material.

Acknowledgements

This project was supported by the National Institute of Health, through Grant Award Number NS095538-02 and a Business Oregon SBIR/STTR matching grant. OCTRI was supported by the National Center for Advancing Translational Science (NCATS), the National Institute of Health (NIH), through Grant Award Number UL1TR002369. We acknowledge S. Malhotra for providing laboratory space for experimentation, S. Jennepalli for assistance with chemical structure visualization, and E. Fraile-Bethencourt for technical assistance with the Wes device.

References

[1]. Zhao GN, Jiang DS, and Li H (2015) Interferon regulatory factors: at the crossroads of immunity, metabolism, and disease, Biochim Biophys Acta 1852, 365–378. [PubMed: 24807060]

[2]. Tamura T, Yanai H, Savitsky D, and Taniguchi T (2008) The IRF family transcription factors in immunity and oncogenesis, Annu Rev Immunol 26, 535–584. [PubMed: 18303999]

[3]. Kulkarni RR, Rasheed MA, Bhaumik SK, Ranjan P, Cao W, Davis C, Marisetti K, Thomas S, Gangappa S, Sambhara S, et al. (2014) Activation of the RIG-I pathway during influenza vaccination enhances the germinal center reaction, promotes T follicular helper cell induction, and provides a dose-sparing effect and protective immunity, J Virol 88, 13990–14001. [PubMed: 25253340]

[4]. Probst P, Grigg JB, Wang M, Munoz E, Loo YM, Ireton RC, Gale M Jr., Iadonato SP, and Bedard KM (2017) A small-molecule IRF3 agonist functions as an influenza vaccine adjuvant by modulating the antiviral immune response, Vaccine 35, 1964–1971. [PubMed: 28279563]

[5]. Pattabhi S, Wilkins CR, Dong R, Knoll ML, Posakony J, Kaiser S, Mire CE, Wang ML, Ireton RC, Geisbert TW, et al. (2015) Targeting Innate Immunity for Antiviral Therapy through Small Molecule Agonists of the RLR Pathway, J Virol 90, 2372–2387. [PubMed: 26676770]

[6]. Es-Saad S, Tremblay N, Baril M, and Lamarre D (2012) Regulators of innate immunity as novel targets for panviral therapeutics, Curr Opin Virol 2, 622–628. [PubMed: 23017246]

[7]. Wilson DR, Sen R, Sunshine JC, Pardoll DM, Green JJ, and Kim YJ (2018) Biodegradable STING agonist nanoparticles for enhanced cancer immunotherapy, Nanomedicine 14, 237–246. [PubMed: 29127039]

[8]. Pencheva N, de Gooijer MC, Vis DJ, Wessels LFA, Wurdinger T, van Tellingen O, and Bernards R (2017) Identification of a Druggable Pathway Controlling Glioblastoma Invasiveness, Cell Rep 20, 48–60. [PubMed: 28683323]

[9]. Bedard KM, Wang ML, Proll SC, Loo YM, Katze MG, Gale M Jr., and Iadonato SP (2012) Isoflavone agonists of IRF-3 dependent signaling have antiviral activity against RNA viruses, J Virol 86, 7334–7344. [PubMed: 22532686]

[10]. Galli R, Paone A, Fabbri M, Zanesi N, Calore F, Cascione L, Acunzo M, Stoppacciaro A, Tubaro A, Lovat F, et al. (2013) Toll-like receptor 3 (TLR3) activation induces microRNA-dependent reexpression of functional RARbeta and tumor regression, Proc Natl Acad Sci U S A 110, 9812–9817. [PubMed: 23716670]

[11]. Corrales L, Glickman LH, McWhirter SM, Kanne DB, Sivick KE, Katibah GE, Woo SR, Lemmens E, Banda T, Leong JJ, et al. (2015) Direct Activation of STING in the Tumor Microenvironment Leads to Potent and Systemic Tumor Regression and Immunity, Cell Rep 11, 1018–1030. [PubMed: 25959818]

[12]. Sivick KE, Desbien AL, Glickman LH, Reiner GL, Corrales L, Surh NH, Hudson TE, Vu UT, Francica BJ, Banda T, et al. (2018) Magnitude of Therapeutic STING Activation Determines CD8(+) T Cell-Mediated Anti-tumor Immunity, Cell Rep 25, 3074–3085 e3075. [PubMed: 30540940]

[13]. Kranzusch PJ, Lee AS, Berger JM, and Doudna JA (2013) Structure of human cGAS reveals a conserved family of second-messenger enzymes in innate immunity, Cell Rep 3, 1362–1368. [PubMed: 23707061]

[14]. Zhao B, Shu C, Gao X, Sankaran B, Du F, Shelton CL, Herr AB, Ji JY, and Li P (2016) Structural basis for concerted recruitment and activation of IRF-3 by innate immune adaptor proteins, Proc Natl Acad Sci U S A 113, E3403–3412. [PubMed: 27302953]

[15]. Tisoncik JR, Korth MJ, Simmons CP, Farrar J, Martin TR, and Katze MG (2012) Into the eye of the cytokine storm, Microbiol Mol Biol Rev 76, 16–32. [PubMed: 22390970]

[16]. Tijono SM, Guo K, Henare K, Palmer BD, Wang LC, Albelda SM, and Ching LM (2013) Identification of human-selective analogues of the vascular-disrupting agent 5,6-dimethylxanthenone-4-acetic acid (DMXAA), Br J Cancer 108, 1306–1315. [PubMed: 23481185]

[17]. Malo N, Hanley JA, Cerquozzi S, Pelletier J, and Nadon R (2006) Statistical practice in high-throughput screening data analysis, Nat Biotechnol 24, 167–175. [PubMed: 16465162]

[18]. McNab F, Mayer-Barber K, Sher A, Wack A, and O'Garra A (2015) Type I interferons in infectious disease, Nat Rev Immunol 15, 87–103. [PubMed: 25614319]

[19]. Ullah MO, Sweet MJ, Mansell A, Kellie S, and Kobe B (2016) TRIF-dependent TLR signaling, its functions in host defense and inflammation, and its potential as a therapeutic target, J Leukoc Biol 100, 27–45. [PubMed: 27162325]

[20]. Sali TM, Pryke KM, Abraham J, Liu A, Archer I, Broeckel R, Staverosky JA, Smith JL, Al-Shammari A, Amsler L, et al. (2015) Characterization of a Novel Human-Specific STING Agonist that Elicits Antiviral Activity Against Emerging Alphaviruses, PLoS Pathog 11, e1005324. [PubMed: 26646986]

[21]. Kato H, Takeuchi O, Sato S, Yoneyama M, Yamamoto M, Matsui K, Uematsu S, Jung A, Kawai T, Ishii KJ, et al. (2006) Differential roles of MDA5 and RIG-I helicases in the recognition of RNA viruses, Nature 441, 101–105. [PubMed: 16625202]

[22]. Nuriel T, Hansler A, and Gross SS (2011) Protein nitrotryptophan: formation, significance and identification, J Proteomics 74, 2300–2312. [PubMed: 21679780]

[23]. Thomsen LL, Ching LM, and Baguley BC (1990) Evidence for the production of nitric oxide by activated macrophages treated with the antitumor agents flavone-8-acetic acid and xanthenone-4-acetic acid, Cancer Res 50, 6966–6970. [PubMed: 2170013]

[24]. Caruso A, Ceramella J, Iacopetta D, Saturnino C, Mauro MV, Bruno R, Aquaro S, and Sinicropi MS (2019) Carbazole Derivatives as Antiviral Agents: An Overview, Molecules 24.

[25]. Saitoh T, Tun-Kyi A, Ryo A, Yamamoto M, Finn G, Fujita T, Akira S, Yamamoto N, Lu KP, and Yamaoka S (2006) Negative regulation of interferon-regulatory factor 3-dependent innate antiviral response by the prolyl isomerase Pin1, Nat Immunol 7, 598–605. [PubMed: 16699525]

[26]. Tarassishin L, and Lee SC (2013) Interferon regulatory factor 3 alters glioma inflammatory and invasive properties, J Neurooncol 113, 185–194. [PubMed: 23512614]

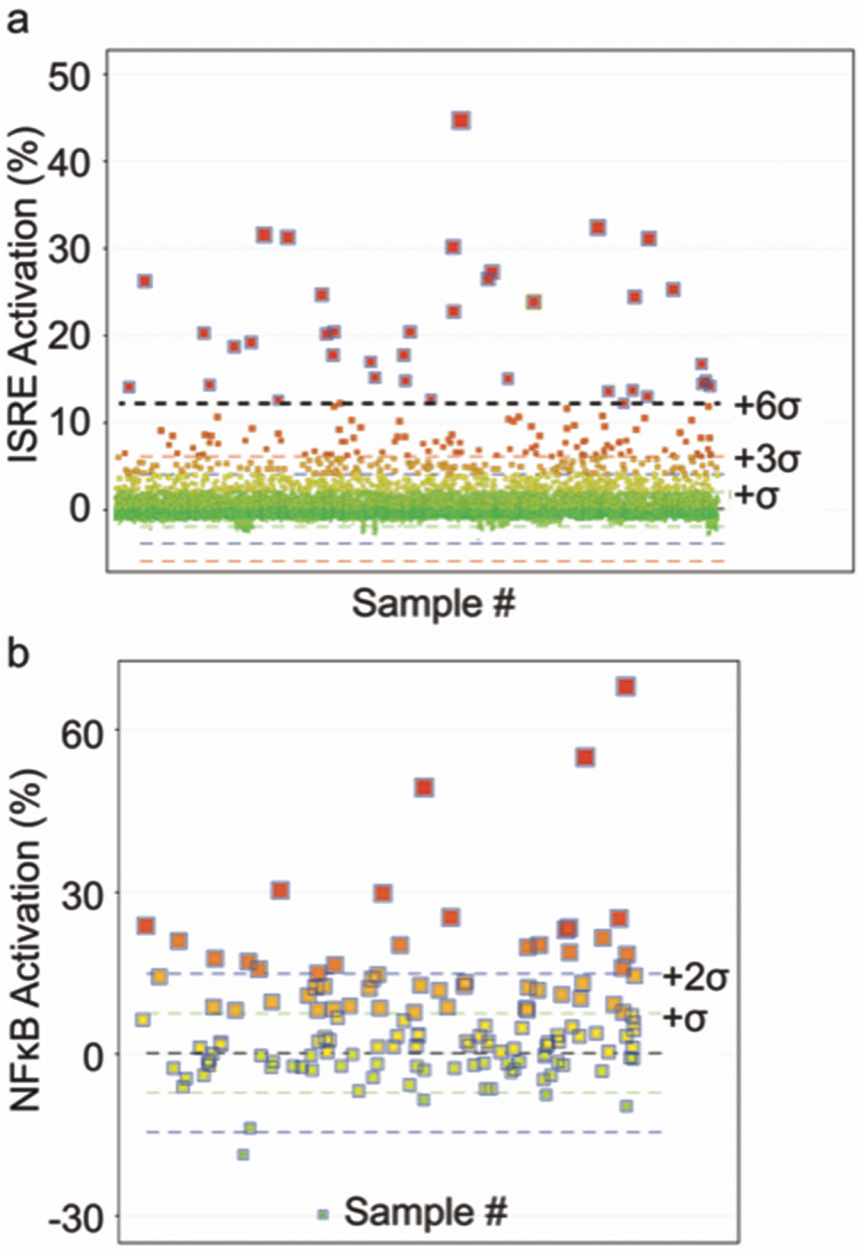

Figure 1. Evaluation of primary screen readout and hit identification.

Data from a representative batch shown in graphs. a) In the PA method data shown here, we normalized the ISRE-coupled luminescence readout to control LPS treatments on each plate to provide a relative percent activation score. In the Zscore method, we performed statistical analysis on raw luminescence data. We selected queries greater than 6σ from the batch mean as hits. b) We performed a counterscreen to select compounds with reduced NFκB-coupled SEAP activation. The graph represents the percent NFκB activation of all combined hits from a representative batch. We set cutoffs for inclusion of hits with NFκB activation above 2σ based on their ISRE/NFκB and ISRE-NFκB signal scores.

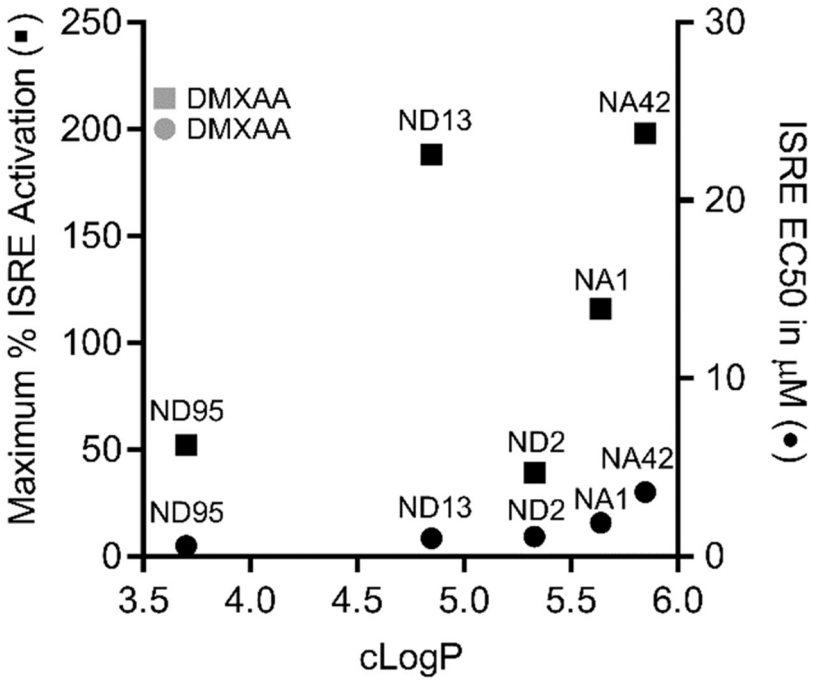

Figure 2.

Comparison of active lead compound properties to the known STING agonist DMXAA. The maximum relative percent activation of ISRE is given on the left axis with data points represented as filled squares. The EC_{50} for ISRE activation is represented on the right axis with data points represented as filled circles. Both DMXAA values are shown in grey, as the compound is active only in mouse. The data for the NA and ND series compounds are from treatment in the human cell model.

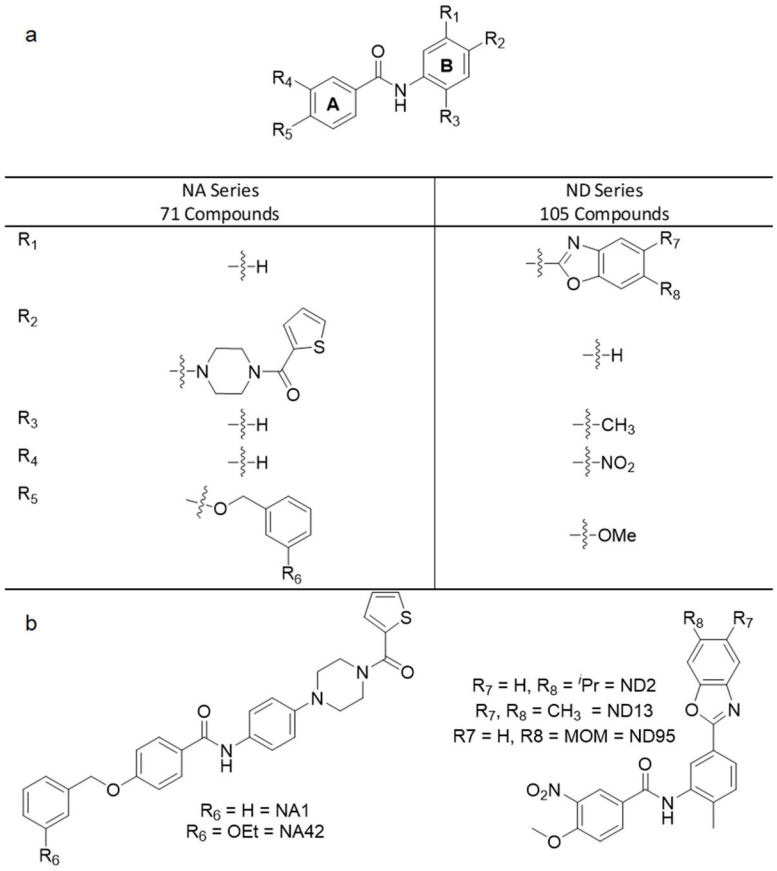

Figure 3.

Chemical structure features of active compounds from series NA and ND. a) The framework for compounds in the structure activity relationship studies is provided with the typical R groups below for active compounds in the NA and ND series. b) The chemical structure of the initial series hit (NA1 and ND2) and their related analogs used in mechanism of action studies are given.

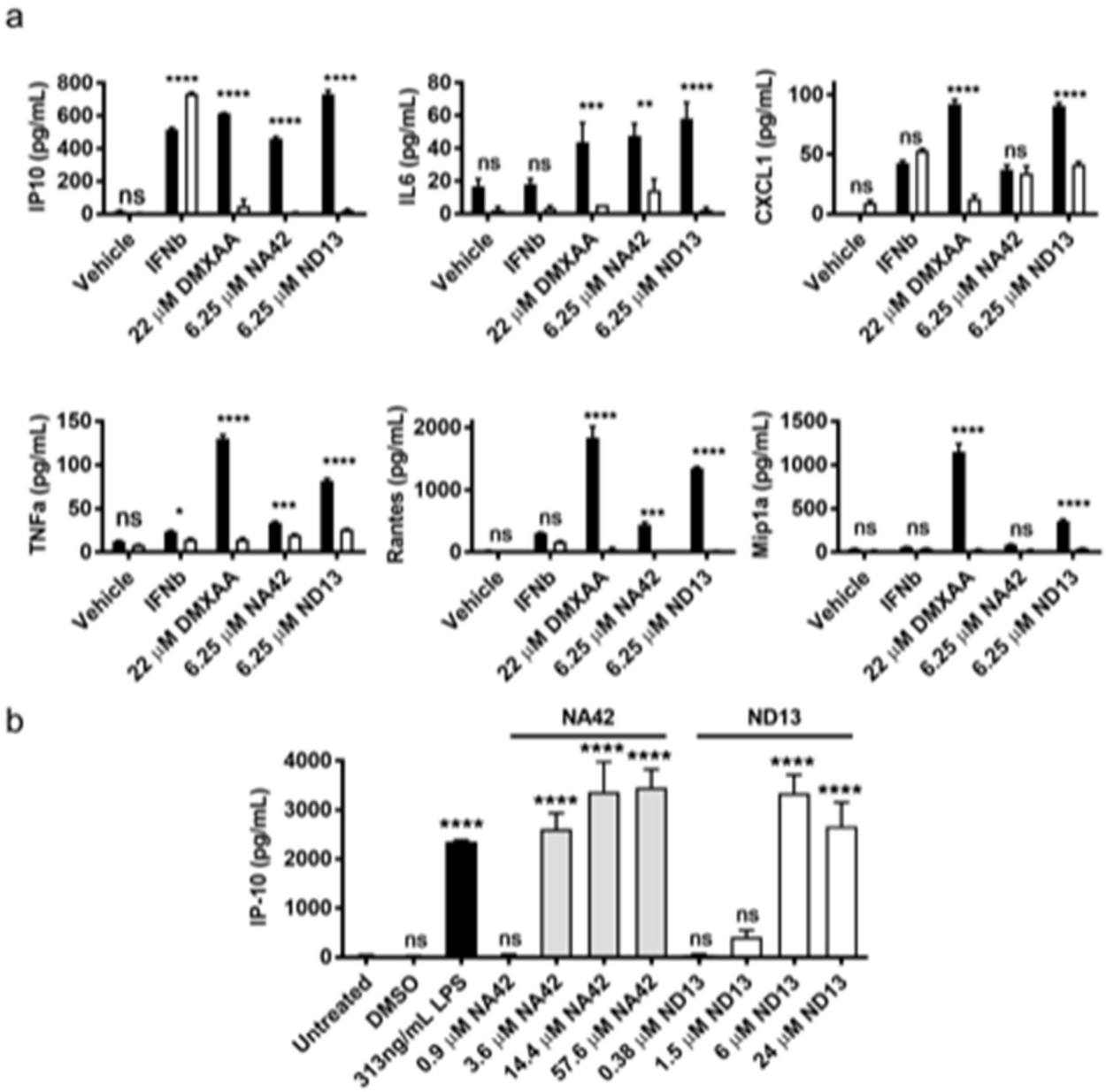

Figure 4.

IRF3 target engagement in ex vivo mouse and human macrophages in response to NA42 and ND13. a) We assessed pro-inflammatory cyto/chemokines from mouse bone marrow-derived macrophages from either wildtype (black bars) or IRF3 deficient mice (white bars). DMXAA, a known IRF3 agonist active in the mouse background, was used as an IRF3-dependent positive control and IFNβ was used as an IRF3 independent control. Both NA42 and ND13 induced cyto/chemokines in a largely IRF3-dependent manner. The p-values for multiple comparisons are designated as >0.1234 (ns), <0.0332 (*), <0.0021 (**), <0.0002 (***), and <0.0001 (****). b) Similar to mouse-derived macrophages, macrophages isolated from whole human blood react to NA42 and ND13 with release of IP10.

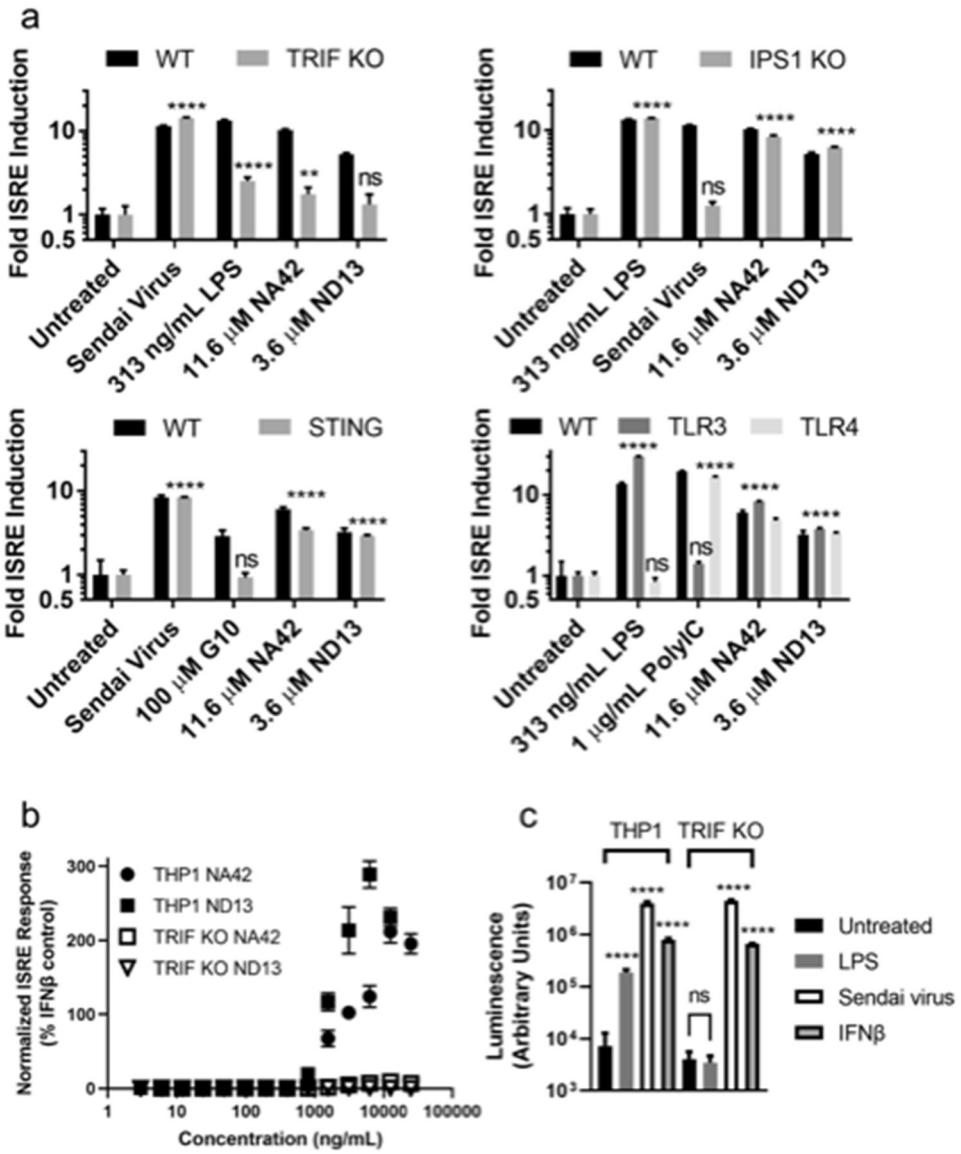

Figure 5.

Biomolecular pathway analysis for ISRE activation by NA42 and ND13. a) We screened a small library of THF cell lines lacking potentially relevant proteins upstream of IRF3 activation (TRIF, STING, IPS1, TLR3 or TLR4). Induction of ISRE was significantly attenuated in the TRIF KO THF cells in response to both NA42 and ND13, while the response in the adaptors IPS1 and STING KO THF cell lines were not affected. This indicates that NA42 and ND13 both activate IRF3 via the adaptor protein TRIF. Interestingly, the receptors TLR3 and TLR4, which are known to signal through TRIF, were not required for ISRE activation by either NA42 or ND13. b) We assessed the activity of NA42 and ND13 in THP1 cells lacking TRIF. Induction of ISRE was lost in the absence of TRIF, suggesting the mechanism of action is consistent across diverse cell types. c) We assessed the reactivity of the WT and TRIF KO THP1 cells with agonists for various receptors to confirm pathway responsiveness. Positive controls for each of the various

knockout cell lines were used (Sendai Virus-IPS1 dependent; G10-STING dependent; LPS-TRIF and -TLR4 dependent; PolyIC-TLR3 dependent). All wildtype treatments resulted in activation statistically different from untreated as determined by 2-way ANOVA at a p-value <0.0001 (****). The p-values listed for TRIF knockout treatments versus untreated are >0.1234 (ns), <0.0021 (**), or <0.0001 (****).

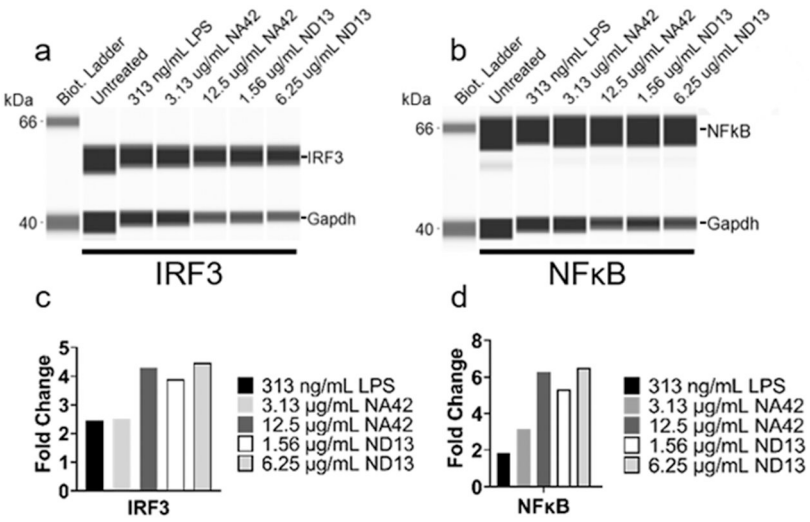

Figure 6.

Evaluation of IRF3 and NFκB protein levels in NA42 and ND13 treated cells. We treated THP1-Dual cells with 313 ng/mL LPS or the indicated concentrations of NA42 and ND13 for 1 hour. Cell culture lysates were analyzed by a capillary electrophoresis western blot method for IRF3 (a) or NFκB (b) using a Wes device. Biot. Ladder stands for biotinylated ladder. c, d) Band densitometry was used to determine the relative amounts of IRF3 and NFκB. Each sample was first normalized to GAPDH and then the amount of IRF3 or NFκB was assessed relative to the untreated control.

Table 1.

Properties of initial hits and major active derivatives. ISRE and NFκB EC_{50} and percent activation values given here were determined in the THP1-Dual human cells. All total polar surface area (tPSA) and calculated LogP (cLogP) values were determined using ChemDraw.

Compound ID	ISRE EC_{50} in μM (Max % Activation)	NFκB EC_{50} in μM (Max % Activation)	tPSA (A^2)	cLogP	Molecular Weight (g/mol)
NA1	1.9 (116)	2.1 (80)	62	5.64	498
NA42	3.6 (198)	3.0 (91)	71	5.85	541
ND2	1.1 (39)	4.5 (4)	112	5.33	445
ND13	1.0 (188)	0.6 (67)	112	4.85	431
ND95	0.6 (52)	1.3 (38)	130	3.7	464